

ARTICLE

Open Access

Fluidic-manipulation-enabled multiplexed dose delivery of RONS by a CAP chip for dose optimization enhancement

Fang Wang^{1,2,3}, Liangyu Zhou⁴, Wei Guo^{1,5}, Haisong Lin¹, Ruotong Zhang¹, Shaolong Kuang³, Yuan Liu¹, Xiaoxue Fan¹, Yau Kei Chan⁴, Hui Deng^{2✉} and Ho Cheung Shum^{1,5,6✉}

Abstract

The plasma-derived reactive oxygen and nitrogen species (RONS) enable cold atmospheric plasma (CAP) to combat cancer and infectious wounds. Achieving therapeutic outcomes with CAP necessitates precise treatment doses. Current CAP devices are constrained by their capability of delivering a single dose to a single sample, limiting dose optimization. We propose a novel “one exposure, multiple-dose delivery” strategy by programming gas flows. This approach facilitates efficient screening of optimal CAP dose by distributing feed gas through boundary-conditioned transport channels to generate multiple, flux-varied gas streams, which ignite plasmas with diverse chemical compositions and dose gradients across samples. Our developed demonstration device, capable of administering three doses to sixteen samples, significantly reduces experimental complexity, particularly when handling large candidate doses or samples for treatment. Leveraging multiplexed treatment, we capably optimize the CAP dose to effectively eradicate the liver cancer cell line of Huh7 and bacteria of *S. aureus* within one exposure. Furthermore, we find manipulating gas flow velocities allows targeted generation of short-lived species. This approach disentangles the roles of short-lived and long-lived RONS in therapeutic applications, offering critical insights into their bio-functional mechanisms. The concept of multiplexed dose treatment with fluidic manipulation promises to catalyze the development of high-efficiency CAP devices and advance research in CAP-based therapies.

Introduction

Plasma is the fourth fundamental state of matter and can be obtained by ionizing gas, rich in ions, electrons, radicals, chemical reactive neutral particles, electromagnetic waves, ultraviolet radiation and electrical fields¹. Under atmospheric conditions, by applying electrical or magnetic fields to oxygen and nitrogen gas, cold atmospheric plasma (CAP) with abundant reactive oxygen species (ROS), including O, O₂⁻, ¹O₂, OH*, O₃, H₂O₂ and reactive nitrogen species (RNS) such as NO, NO₂⁻,

NO₃⁻, OONO⁻ are produced². Well documented literature has demonstrated that, through generating RONS, CAP can destroy cellular antioxidant system, damage mitochondria and genetic material, and ultimately induce cell death^{3–5}. Additionally, CAP can etch bacterial cell walls, induce lipid peroxidation leading to irreversible DNA and protein damage, and disrupt the structural integrity of biofilms targeting microorganisms within^{6,7}. Moreover, CAP treatment has been shown to recruit inflammatory cells to wound sites, induce pro-inflammatory effects, and activate fibroblast to regulate collagen synthesis, angiogenesis, and wound remodeling^{8,9}. These effects suggest that CAP holds promise as an effective therapeutic modality to combat cancer, treat bacterial infections and promote wound healing. The therapeutic effects of CAP-based therapy are highly dependent on the administered dose^{10,11}. Depending on

Correspondence: Hui Deng (dengh@sustech.edu.cn) or Ho Cheung Shum (ashum@hku.hk)

¹Department of Mechanical Engineering, The University of Hong Kong, Hong Kong SAR, China

²Department of Mechanical and Energy Engineering, Southern University of Science and Technology, Shenzhen, China

Full list of author information is available at the end of the article

© The Author(s) 2025



Open Access This article is licensed under a Creative Commons Attribution-NonCommercial-NoDerivatives 4.0 International License, which permits any non-commercial use, sharing, distribution and reproduction in any medium or format, as long as you give appropriate credit to the original author(s) and the source, provide a link to the Creative Commons licence, and indicate if you modified the licensed material. You do not have permission under this licence to share adapted material derived from this article or parts of it. The images or other third party material in this article are included in the article's Creative Commons licence, unless indicated otherwise in a credit line to the material. If material is not included in the article's Creative Commons licence and your intended use is not permitted by statutory regulation or exceeds the permitted use, you will need to obtain permission directly from the copyright holder. To view a copy of this licence, visit <http://creativecommons.org/licenses/by-nc-nd/4.0/>.

the treatment dose, CAP exposure can induce cell growth, cell senescence, and cell death¹² (Fig. 1a). Furthermore, identical doses can elicit different responses in cancerous cells and healthy cells¹³. For instance, the lethal dose for cancer cells exceeds that for normal cells, creating a narrow window for optimizing the dose to eradicate cancerous cells while minimizing harm to healthy cells¹⁴. Similarly, in treating infected wounds, the applied CAP dose should be carefully controlled to achieve effective bactericidal effects while ensuring biosafety. To pinpoint the appropriate dose for specific disease treatment, CAP exposure devices incorporating multiplexed dose delivery channels and enhanced dose optimization efficiency are expected. However, currently, available devices with such capabilities are limited^{15–19}, posing a longstanding challenge to the clinical application of CAP-based therapy.

Due to their operational convenience and ability to penetrate narrow space, CAP-jet^{20–22} devices are widely utilized for sample radiation. The dose modulation primarily hinges on the input power, discharge distance, dielectric barrier properties, exposure duration, gas flows, and radiation distance²³. Once the exposure parameters are established, such as setting the feeding gas velocity to adjust the treatment dose, the dimensionally constrained plasma jet can administer only one dose to one sample per exposure (Fig. 1b). This “single-sample, single-dose” treatment approach relies on trial and error, placing a heavy burden on researchers to traverse a vast experimental parameter space. For instance, in a small-scale test involving 4 samples (A, B, C, D), 5 candidate doses, and 4 independent experiments per group, up to 80 experiments are required to identify the optimal dose among the 5 candidate gas flow velocities (Q_1, Q_2, Q_3, Q_4, Q_5) for the 4 samples (Fig. 1c).

Targeting to streamline the selection of optimal doses in experiments, we propose a novel concept: delivering multiplexed doses within a single treatment session. The design involves a top-down engineered feeding gas fluidic field that programs multiple flux-various gas streams to provide multiplexed-dose channels. Instead of igniting a single feeding gas stream directly, multiple streams are injected into the discharge cavity through gas inlets (Fig. 1d). Gas transport channels establish specific boundary conditions of the fluidic field to reshape the original injected gas streams and produce flux-diverse gas flows²⁴ (Fig. 1e: Q_{iv}, Q_{iiv}, Q_{iii}). When flowing through the discharge electrodes, the redistributed gas streams undergo diverse chemical reactions and ignite chemistry-diverse plasmas²⁵. As a demonstration, these plasmas can administer three different treatment doses to the loaded bio-samples, effectively enhancing dose optimization efficiency by at least threefold (Fig. 1e). For the same test exhibited in Fig. 1c, the prototype device requires only eight experimental cycles to fulfill the dose optimization

task (Fig. 1f). With the increase of the candidate samples, the advantages of the multiplexed dose delivery device in alleviating the experiment burden stand out (Fig. 1g). Furthermore, our design allows flexible configuration of gas inlets and transport channels to accommodate varying numbers of dose levels and sample wells for specific research, further mitigating experimental burdens. The multiplexed dose delivery modality significantly improves dose optimization efficiency and facilitates a comprehensive study of biophysical mechanisms of CAP-based therapies by examining diverse sample responses across a broad range of doses. The concept of manipulating the gas fluidic field to achieve multiplexed dose delivery will inspire the development of intelligent and digital CAP exposure devices, benefiting both fundamental research and clinical administration of CAP-based therapy.

Results and discussion

Manipulate fluidic field to produce velocity-diverse gas streams for multiplexed dose delivery

Three dimensions of the gas flow model were established and calculated in the COMSOL Multiphysics (version 6.0) platform to simulate the transformation of the fluidic field for producing velocity-varied gas streams. A quarter model was selected to simplify calculations (Fig. 2a). Feed gases enter the device through gas inlets and disperse via transport channels categorized into Group 1 (green channels), Group 2 (yellow channels), and Group 3 (blue channels) (Fig. 2a). Upon injection, the feed gases diffuse along the injection axis and subsequently spread across the entire space (Figs. 2b and S1 and Movie 1). Gas diffusion velocities decrease with the increment of the diffusion distance²⁴. Initially, distance-dependent diffusion causes a greater accumulation of gases above Group 1 channels, followed sequentially by Group 2 and Group 3 channels (Fig. S2). However, Group 2 channels can capture adjacent two injected gas streams, whereas Group 1 and Group 3 channels can only capture one gas stream that originates from gas inlets II, IV, VI, and VIII (Fig. S3). As diffusion distance increases, overlay diffusion surpasses distance-dependent diffusion and dominates gas distribution. Correspondingly, Group 2 channels witness the highest gas flow velocity at the entrance of the transport channel (Fig. 2c-i).

To enter the transport channels, the feed gas converges into high-speed narrow streams. Due to variations in gas entering velocity and angle, the reproduced three groups of gas streams exhibit distinct distribution topography in the cross-section: Group 1 streams occupy the lower-left quadrant, Group 2 streams occupy either the lower-right or upper-left quadrant, and Group 3 streams nearly fill the entire channel (Fig. S4). After entering the transport channels, the suddenly enlarged space decelerates the gas flows (Fig. 2c-ii). Since Group 3 streams maintain a

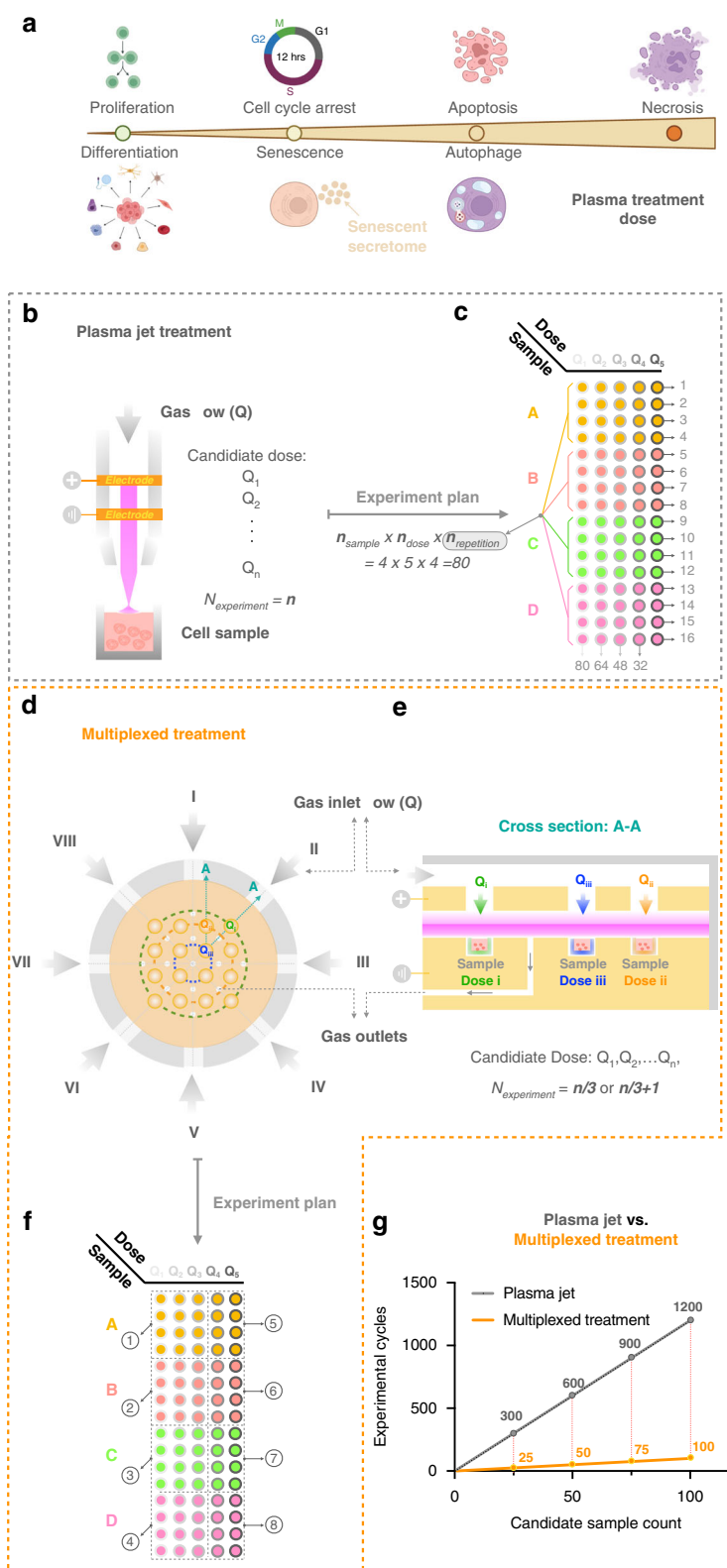


Fig. 1 Overview of multiplexed dose delivery for efficient CAP dose optimization. **a** The critical role of CAP dose in eliciting different cell behaviors. **b** Schematic of the conventional single-dose, single-sample treatment modality by a plasma jet device. **c** Experimental design for a small-scale test utilizing a plasma jet device. **d, e** Conceptual framework of multiplexed dose delivery with fluidic manipulation. **f** Experimental design for a typical small-scale test utilizing the multiplexed treatment device. **g** Significance of the multiplexed dose delivery device in reducing experiment cycles with increased candidate samples (e.g., three candidate doses and four repetitions per experiment)

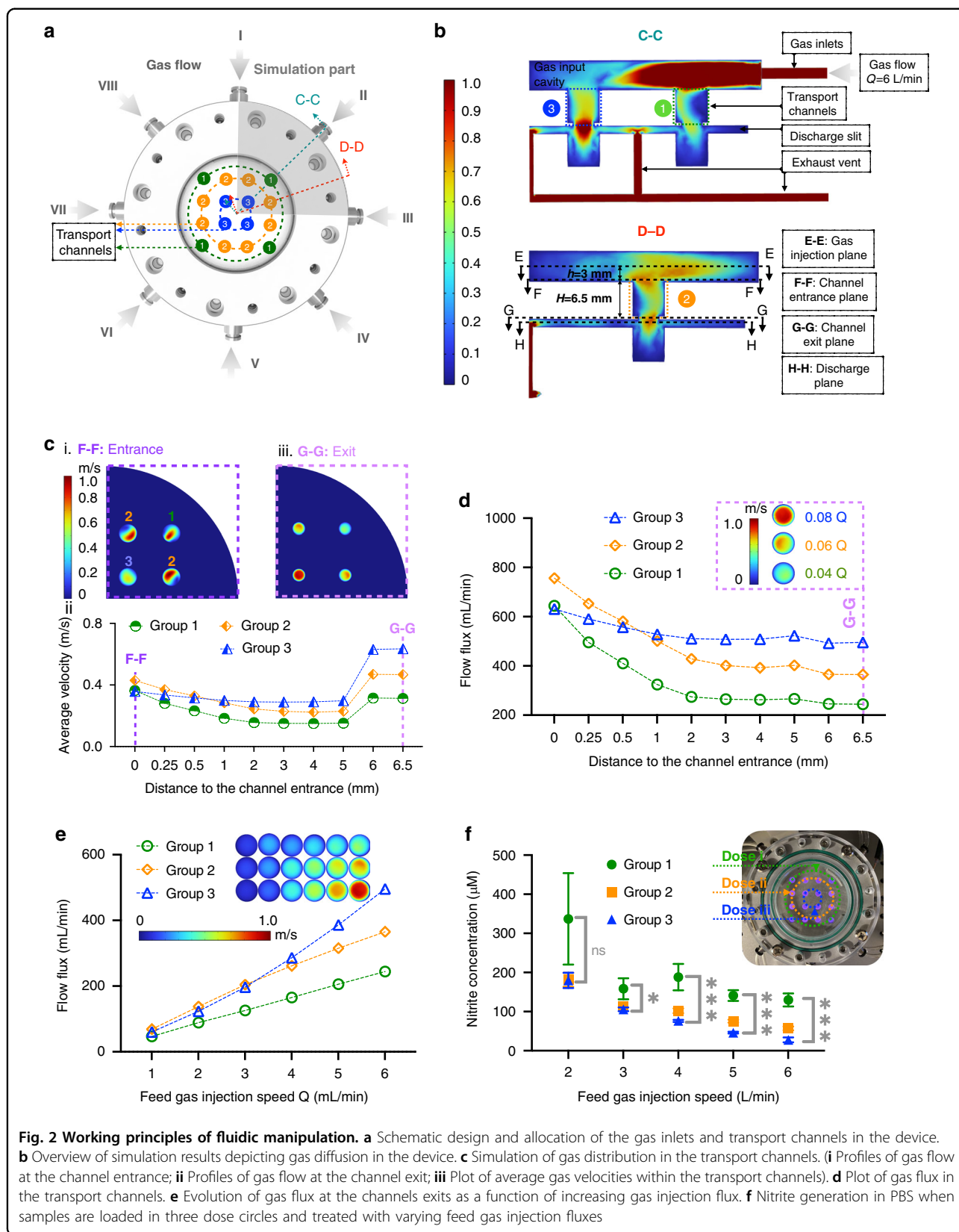


Fig. 2 Working principles of fluidic manipulation. **a** Schematic design and allocation of the gas inlets and transport channels in the device. **b** Overview of simulation results depicting gas diffusion in the device. **c** Simulation of gas distribution in the transport channels. (i) Profiles of gas flow at the channel entrance; (ii) Profiles of gas flow at the channel exit; (iii) Plot of average gas velocities within the transport channels). **d** Plot of gas flux in the transport channels. **e** Evolution of gas flux at the channels exits as a function of increasing gas injection flux. **f** Nitrite generation in PBS when samples are loaded in three dose circles and treated with varying feed gas injection fluxes

diameter similar to that of the channel, their flow velocity is less reduced and becomes the highest at the channel exit, followed by Group 2 and then Group 1 channels (Fig. 2c-iii). At a distance of 0.5 mm from the channel exit, gas flow velocities experience a significant increase due to a 2 mm reduction in channel diameter, necessary for inserting the dielectric barrier sheet to prevent arc discharge. Within the discharge slit, gas streams start to move from the transport channels to the exhaust vents while maintaining the formed gas velocity gradient (Fig. S5). Besides, the fluidic field is resistant to the device dimension variations (Fig. S6). Provided the height of transport channels is larger than 3.5 mm, the fluidic field remains stable, indicating good tolerance towards machining and assembly errors.

When feed gases are injected into the device at a flow flux of $Q = 6$ L/min, the flow fluxes at the channel exit are 234.6 mL/min (0.04Q) for Group 1 channels, 350.4 mL/min (0.06Q) for Group 2 channels, and 475.8 mL/min (0.08Q) for Group 3 channels (Fig. 2d). Theoretically, the excited plasma chemistry can be associated with gas flow velocities²⁶. The differentiated flow flux at the channel exit predicts that the fluidic field can be programmed by redistributing the injected gases to excite chemistry-diverse plasmas. Moreover, varying the feed gas injection flux could further modulate these flow flux differentials: higher injection fluxes lead to more pronounced differences (Fig. 2e). As aforementioned, plasma treatment dose can be presumably evaluated based on the synergy of the generated reactive species, electromagnetic waves, and ultraviolet radiation. However, accurately quantifying these reactive species poses challenges in defining treatment doses based on clear plasma chemistry. Nitrite is a typical plasma-produced long-lived species and can be easily quantified²⁷, thus here we consider it as a potential indicator to imply the dose discrepancy. For instance, when gas injection flux exceeds 3 L/min, a 1-min plasma treatment can result in 3 concentrations of the nitrite in 100 μ L PBS (Fig. 2f). Consequently, the 3 groups of gas streams capably produce chemistry-diverse plasmas for multiplexed dose delivery.

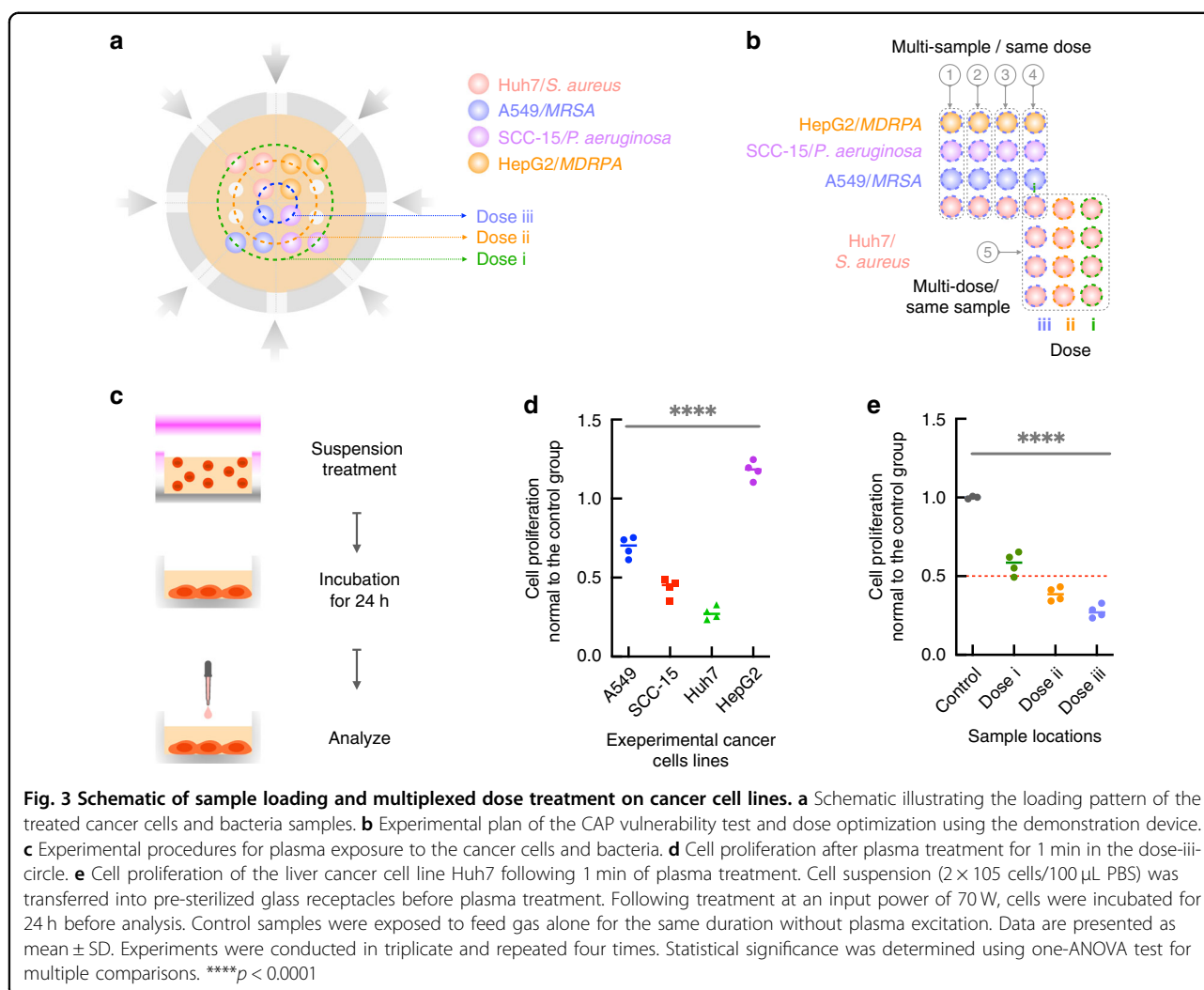
Demonstration of plasma-vulnerability evaluation and dose optimization by multiplexed dose treatment on cancer cells and bacteria

Selective-killing tumor cells represents the most attractive biomedical application of CAP^{28,29}. Although radiotherapy and chemotherapy can be employed to fight cancer, their indiscriminate killing of healthy and cancerous cells causes severe adverse effects harming the patient's body^{30,31}. In contrast, CAP can preferentially kill tumor cells by destroying redox homeostasis, without giving rise to side effects or inducing any drug resistance^{32,33}. When employed adjunctively, CAP can even

re-sensitize the resistant cells to chemotherapy^{34,35}. Additionally, CAP can effectively eradicate bacteria, enabling the treatment of bacteria-infected disease^{36,37}. Clinically, broad-spectrum antibiotics are predominantly used to treat keratitis³⁸, periodontitis³⁹, and infected wounds⁴⁰. However, excessive antibiotic use can promote drug-resistant bacteria strains, leading to treatment failures and exacerbating infections⁴¹. In contrast, CAP eliminates bacteria by the synergistic action of plasma-produced reactive oxygen and nitrogen species, which are less likely to induce drug resistance³⁷. Moreover, CAP can enhance therapeutic effects by promoting cell proliferation for wound healing^{42–44}. Since different cancer cells and bacteria strains exhibit varying susceptibility to plasma treatment⁴⁵, CAP-based therapy is particularly effective against plasma-vulnerable cancers and bacteria-induced disease, with optimal treatment doses tailored to achieve therapeutic effects. Here we radiate four types of cancer cell lines (A549, SCC-15, Huh7, HepG2) and four strains of bacteria (*S. aureus*, MRSA, *P. aeruginosa*, MDRPA) with our prototype device to analyze their susceptibility to CAP and explore the optimal dose.

Different samples were loaded onto the same dose circle to screen for the more sensitive cancer type, whereas the same samples were placed on different dose circles to optimize the treatment dose (Fig. 3a). Following this sample loading pattern, five experiment cycles will be sufficient to identify the most vulnerable cancer type or bacteria strain and determine the applicable treatment dose, which is more than five times faster than with traditional plasma jet devices (27 experiment cycles required) (Fig. 3b). Since low feeding gas flux cannot effectively distinguish the three doses (Fig. 2f), the gas injection flux of $Q = 4$ L/min was selected to ignite the chemistry-various plasmas for multiplexed dose delivery. As no standard or universally accepted dose definition has been established yet, we follow the routines of characterizing the dose based on plasma-ignition input parameters in our confirmatory experiments (Table 1). Cell suspensions are transferred to pre-sterilized glass receptacles for plasma exposure, followed by a 24-h incubation in 6-well plates for subsequent analysis (Fig. 3c).

The Huh7 liver cancer cell line demonstrates high sensitivity to CAP with a proliferation rate of 27.6% after 1-min treatment, followed by the SCC-15 tongue cancer cell line at 43.58%, and the A549 lung cancer cell line at 69.36% (Fig. 3d). In contrast, the HepG2 cell line exhibits relative resistance to CAP, showing a significantly increased proliferation rate of 117.9%. CAP treatment results in clear cell shrinkage and detachment of A549, Huh7, and SCC-15 cells (Fig. S7). When considering different doses, dose iii treatment results in a proliferation rate of 27.5% for Huh7 cells, followed by dose ii (38.6%), and dose i (58%) (Figs. 3e and S8). Clearly, the Huh7 cell

**Table 1 Dose definition parameters**

	Dose i	Dose ii	Dose iii
Power frequency	13.56 MHz		
Discharge intensity	1.99 W/cm ²		
Dielectric barrier	Quartz (0.5 mm in thick)		
Discharge distance	1.5 mm		
Gas flow rate	165 mL/min (0.04Q)	261 mL/min (0.065Q)	286 mL/min (0.07Q)
Gas mixture	Helium/Nitrogen (0.2%)		
Treatment duration	1 min		

line is the most vulnerable to CAP and appears promising for plasma-based cancer therapy among the tested four cell lines. Evaluating treatment doses based on cell proliferation rates and following a clinical dose evaluation

standard akin to a 50% lethal rate⁴⁶, dose iii emerges as the most suitable. In terms of bacterial treatment, 1-min plasma exposure kills 100% of *P. aeruginosa* and MDRPA, while *S. aureus* and MRSA show varying degrees of resistance to CAP, with a proliferation rate of 22.9% and 70.3%, respectively (Fig. 4a, b). Among the doses tested, dose iii results in a proliferation rate of 22.9% for *S. aureus*, followed by 35.5% for dose ii, and 66.5% for dose i (Fig. 4c). These findings indicate that *P. aeruginosa* and MDRPA are highly susceptible to plasma treatment, making them suitable targets for CAP-based bactericidal therapy. Meanwhile, CAP-based therapy shows promise for treating *S. aureus* infections, as 1-min radiation (dose iii) achieves a proliferation rate of 22.9%, with proliferation rates between dose i and dose ii approaching 50%.

When the potentially effective dose outranges the current set 3-level doses (1 min/70 W), we have options to increase the input power or extend the treatment duration (conventional dose modulation approach) to elevate

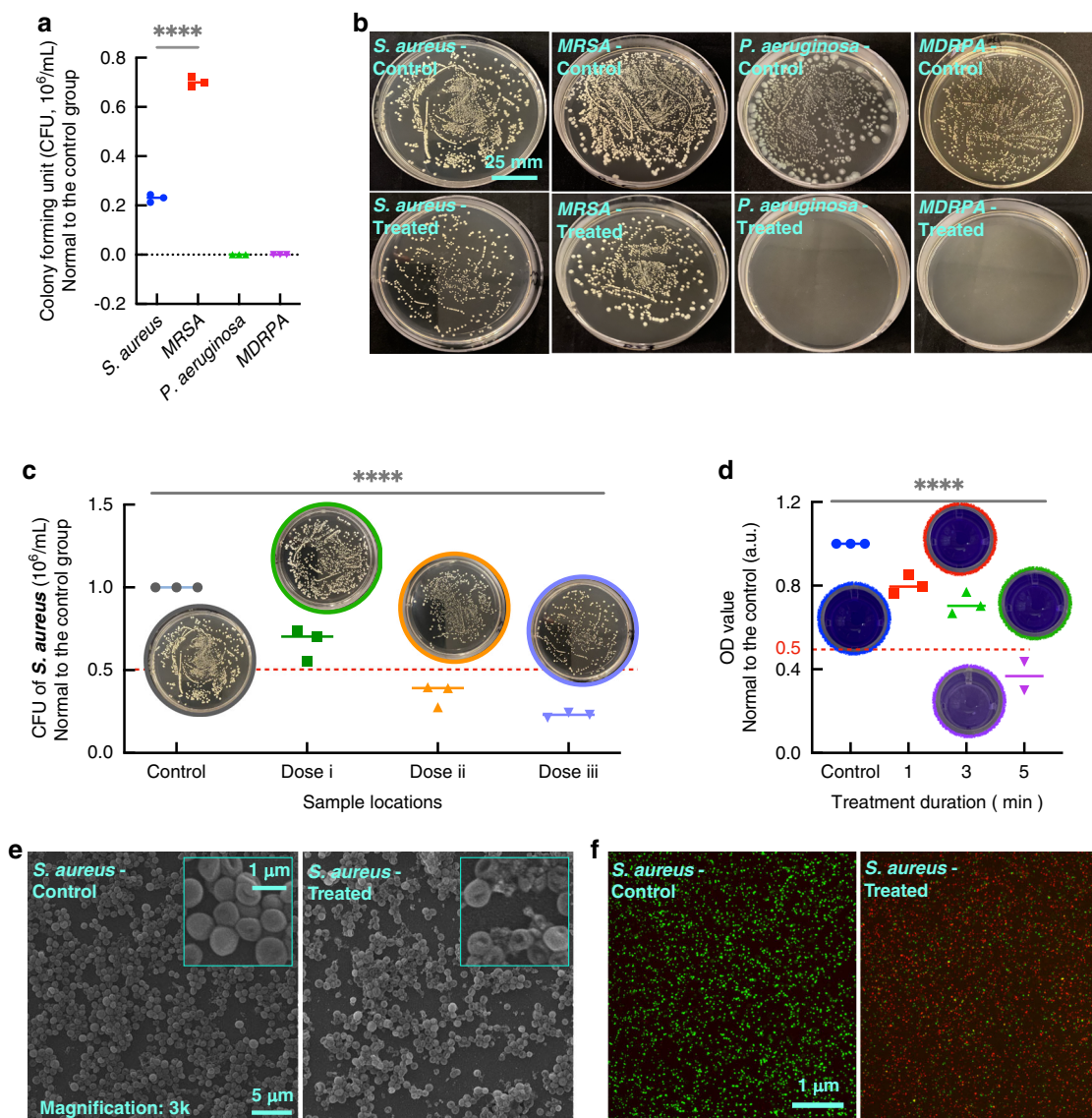


Fig. 4 Multiplexed dose treatment on various bacteria. **a** Viability of *S. aureus*, MRSA, *P. aeruginosa*, and MDRPA following CAP treatment. Samples were prepared by diluting the original bacteria culture media in PBS to form a 10⁶ CFU/mL suspension. 100 μ L of sample was transferred to glass receptacles and treated with CAP for 1 min at an input power of 70 W within the dose iii circle. **b** Remaining colony-forming units of the bacteria post-CAP treatment. **c** Viability and remaining colony forming units of *S. aureus* after CAP treatment. *S. aureus* suspension (10⁶ CFU/mL) were simultaneously loaded into the three dose circles and subjected to CAP treatment for 1 min at an input power of 70 W. **d** Viability of *S. aureus* biofilm following CAP treatment. A 100 μ L sample of *S. aureus* suspension (10⁸ CFU/mL) was placed in the dose iii circle and exposed to CAP for 1, 3, and 5 min at an input power of 70 W. Treated samples were incubated for 48 h and stained with crystal violet to assess biofilm growth. **e** SEM image of *S. aureus* biofilm. A 100 μ L *S. aureus* suspension (10⁸ CFU/mL) was incubated on the coverslips for 24 h to form the biofilm. The biofilm was then treated with CAP for 1 min at an input power of 70 W within the dose iii circle. **f** Lived-dead assay of *S. aureus* biofilm post-plasma treatment. A 100 μ L *S. aureus* suspension (10⁸ CFU/mL) was incubated in glass receptacles for 24 h to form the biofilm. The biofilm was exposed to CAP for 5 min at an input power of 70 W within the dose iii circle. Data are presented as mean \pm SD. Experiments were conducted in triplicate and repeated two or three times. Statistical significance was determined using either one-way ANOVA test or *t* test for multiple comparisons. *****p* < 0.0001

overall dose levels and synergy with multiplexed treatment for dose optimization. Biofilms, which shield encapsulated bacteria from plasma-produced reactive species, require a higher 50% lethal CAP dose for eradication compared to planktonic bacteria⁴⁷. To demonstrate

the traditional dose optimization, *S. aureus* biofilm was exposed to plasma for 1 min, 3 min, and 5 min on the dose iii circle. The violet-staining reveals biofilm growth reductions of 20% with 1-min treatment, 28.6% with 3-min treatment, and 63.3% with 5-min treatment

(Fig. 4d). Brief treatments (1 min) reduce biofilm coverage, causing bacteria shrinkage and fragmentation (Fig. 4e), while longer treatments (5 min) lead to over 90% bacteria death (Fig. 4f). The treatment duration for achieving a 50% proliferation dose in *S. aureus* biofilm is estimated to be around 4 min (Fig. S9). Precise treatment doses can be determined by placing samples on the three-dose circles and exposing them to plasma for 4 min. This flexible combination of innovative multiplexed dose treatment and traditional dose modulation facilitates dose optimization tasks. Multiplexed dose treatment enables efficient testing of target cell lines and bacteria strains for CAP susceptibility and facilitates optimizing applicable treatment doses, advancing the clinical application of CAP-based therapies. The distinct growth inhibition and eradication effects observed with CAP treatment indicate that different dose regimens can induce varying biological responses, exerting different levels of pressure on the samples. Multiplexed dose treatment aids in effectively analyzing sample responses under diverse dose conditions, enhancing understanding of the CAP anti-cancer mechanisms.

Gas flow velocity plays dual roles in producing RONS for cancerous cells eradication

The anti-cancer and bactericidal effects of CAP can be attributed to the produced reactive oxygen (O , O_2^- , 1O_2 , OH^* , O_3 , H_2O_2) and nitrogen species (NO , NO_2^- , NO_3^- , $OONO^-$)⁴⁸. Due to the high reactivity, the short-lived species (O , O_2^- , 1O_2 , OH^* , O_3 , NO , $OONO^-$) can only diffuse over a limited distance, often failing to reach the target samples. Consequently, the responses of treated bio-samples are dominated by long-lived species such as NO_2^- , NO_3^- , and H_2O_2 ⁴⁹. Given that our samples are suspended in PBS, the short-lived species are likely neutralized by the liquid barrier, leaving the long-lived species primarily responsible for cell eradication. Thus, theoretically, cell suppression should increase with higher levels of NO_2^-/NO_3^- and H_2O_2 generation⁵⁰. However, in our experiment, a higher concentration of NO_2^- does not aggravate cell suppression; instead, it results in a relatively higher rate of cell proliferation. For instance, 1.5-min plasma treatment of 100 μ L PBS yielded 150 μ M NO_2^- for samples placed in dose i circle, 95 μ M for dose ii, and 69 μ M for dose iii (Fig. 5a). In contrast, under the same plasma treatment conditions, the A549 lung cancer cells suspended in 100 μ L PBS exhibited a proliferation rate of 85% for dose i, 60% for dose ii, and 56% for dose iii (Fig. 5b). This result suggests that the long-lived species of NO_2^-/NO_3^- and H_2O_2 , are not the main contributors to inhibiting cell growth. When the short-lived species are removed by treating the cells with plasma-activated PBS, the cell proliferation rates across the three-dose circles approximate the same value of 90% (Fig. 5c).

Consequently, we hypothesize that the unexpected cell growth inhibition (with a dose-dependent trend: dose i > dose ii > dose iii) is attributed to the short-lived species.

To substantiate this hypothesis, we conduct comparative tests to exclude other potential factors. The cell proliferation rates of both control and experimental groups remained consistent when cells were treated with blowing gas without CAP ignition (Fig. S10A). A 1-min CAP treatment only evaporated 2.25% suspension (2.25 μ L), leaving sufficient PBS (97.75 μ L) to suspend and protect the cells (Fig. S10B). The pH value remained around 7.2, indicating that CAP treatment did not acidify the cell suspension to suppress cell growth (Fig. S10C). When cells were shielded with a shelter (Fig. S10D) to block reactive species, allowing only the transmission of UV & electromagnetic waves (UV-transmissible quartz shelter) or solely electromagnetic waves (UV-opaque glass shelter), the CAP treatment resulted in a comparative cell proliferation rate to the control group (Fig. S10E). Cell growth inhibition was not observed when cells were treated with a parallel-electrode-established uniformly distributed electric field (Fig. S11A) without plasma excitation (Fig. S11B). These results support the hypothesis that short-lived species play a crucial role by excluding the functions of gas blowing, evaporation, acidification, electromagnetic waves, UV, and electrical fields in suppressing cell growth.

According to the design concept, the different gas flow velocities are exclusively exploited to distinguish plasma treatment doses. In principle, the gas flow velocity can influence both the plasma ionization coefficient and the interaction between the produced species and the sample⁵¹. Within appropriate intervals, a higher gas flow velocity can intensify plasma species by increasing electron density but may reduce the interaction duration between species and sample²⁵. However, for the short-lived species with extremely short lifespans (nano/microseconds), increasing gas flow velocity does not diminish the interaction opportunity between these species and the samples⁵². Thus, their production is primarily determined by plasma ionization, and their evolution should correspond with changes in gas flow velocities. In contrast, long-lived species either derive from solvents of short-lived species or result from chemical reactions (seconds/minutes) between short-lived species and the sample. Consequently, their concentrations are synergistically influenced by the yield of their precursor short-lived species and the interaction duration between species and sample⁵³.

In our experiment, increased gas flow velocity facilitates the production of short-lived species such as OH , N_2 , H , O , and He (Figs. 5d and S10), but it may restrict nitrite generation by reducing the interaction duration of precursor species with samples. The shortened interaction

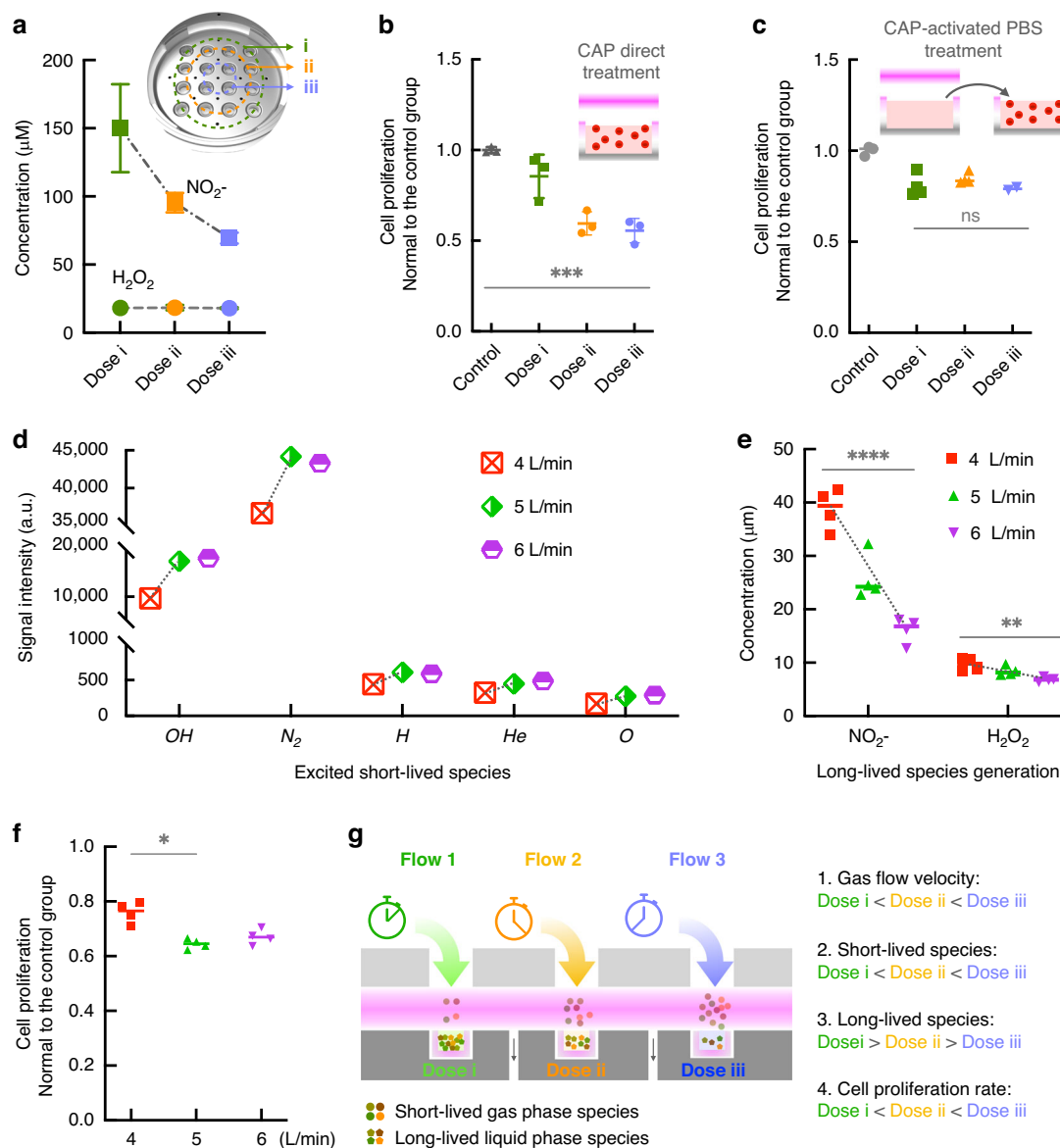


Fig. 5 Identifying the cell growth inhibition factors. **a** Generation of Long-lived species in 100 μL PBS following plasma treatment for 1.5 min at an input power of 70 W. **b** Proliferation of the lung cancer cells (A549) after plasma treatment for 1.5 min. **c** Proliferation of lung cancer cells treated with plasma-activated PBS (The PBS was exposed to plasma for 1.5 min). **d** Generation of short-lived species with increased feed gas injection speed. **e** Generation of long-lived species with increased feed gas injection speed. **f** Cell proliferation rate as a function of increased feed gas injection speeds. **g** Schematic illustrating the dual roles of gas flow velocity in producing long-lived and short-lived species. Data were presented as mean \pm SD. All experiments were conducted in triplicate and repeated three or four times. Statistical significance was determined using either a *t* test or a one-way ANOVA. * $P < 0.05$, ** $P < 0.005$, *** $P < 0.0005$, **** $P < 0.0001$

duration affects nitrite generation more significantly than the enhanced production of precursor short-lived species, resulting in decreased nitrite concentrations with increasing gas flow velocity (Fig. 5e). Since the interaction duration does not affect short-lived species generation, both their production and interaction with samples are intensified, thereby enhancing cell eradication with increasing gas flow velocity. (Fig. 5f). For a feed gas

injection flux of $Q = 4$ L/min, the gas flow fluxes for the three doses are dose iii (0.07 Q) > dose ii (0.065 Q) > dose i (0.04 Q) (Table 1). Based on the above discussions and experimental verifications, the yield of short-lived species is expected to be positively correlated with gas flow velocities: dose iii > dose ii > dose i. This trend aligns closely with dose-dependent cell growth inhibition: dose iii (56%) < dose ii (60%) < dose i (85%). Interestingly, despite

of the challenge short-lived species face in crossing the liquid barrier, our results indicate they still have a chance to impact the cells, as the long-lived species alone cannot effectively suppress cell growth. Consequently, the gas flow velocity can be finely tuned to either highlight the role of short-lived species with higher feed gas flow velocities or emphasize the function of the long-lived species with lower feed gas flow velocities (Fig. 5g). This approach can disentangle the roles of short-lived and long-lived RONS in therapeutic applications, offering critical insights into their bio-functional mechanisms.

Conclusion

To improve dose optimization for mechanisms understanding and clinical application of plasma-based therapy, we proposed the concept of manipulating the fluidic field to achieve multiplexed dose delivery within one exposure. By programming the gas flows with boundary-conditioned channels, we developed the 3-dose-16-sample demonstration device, which can enhance dose optimization by more than tenfold compared to the traditional plasma jet. Leveraging the multiplexed dose treatment, we efficiently identified the vulnerability towards CAP treatment of four types of cancer cell lines and bacteria: Huh7>SCC15>A549>HepG2 (cancer cell lines), *P. aeruginosa*/MDRPA>*S. aureus*>MRSA (bacteria) and determined the correspondingly optimal treatment dose of Huh7 (dose i) and *S. aureus* (between dose ii and dose iii). Furthermore, we found that short-lived RONS could overcome the liquid barrier to suppress cell growth and the gas flow velocity played dual roles in producing the short-lived versus long-lived RONS. Higher gas flow velocity facilitated the production of short-lived species, while lower gas flow velocity preferentially produced long-lived species in liquid.

The concept of multiplexed dose delivery with fluidic manipulation will inspire the development of high-efficiency plasma exposure devices for the optimization of treatment doses, especially in the situation of numerous candidate samples or doses. The analyzed sample responses under a wide range of treatment doses can establish a valuable correlation, helping understand the RONS functional mechanisms and improve the clinical application of CAP-based therapy. The dual role of the feed gas flow velocity allows us to decouple the effects of the short-lived versus long-lived RONS, providing critical insights into the bio-functional mechanisms of the RONS. Currently, even though the significant role of the short-lived species is identified, the specific species evolution processes and functional mechanisms remain unclear and will be investigated in the future. Besides, a clinical-available therapeutical instrument will be adapted from this in-vitro research device to deliver the optimized treatment dose achieving precise plasma-based therapy.

Materials and methodologies

Cell culture, plasma treatment, and proliferation characterization

The human liver cancer cell line of Huh7 and HepG2, lung cancer cell line of A549, and fibroblast NIH3T3 cells were cultured in a 100 mm culture dishes with high-glucose DMEM (21063029, Gibco), 10% fetal calf serum (A4766801, Gibco), and 1% penicillin-streptomycin (15140122, Gibco). The tongue cancer cell line of SCC-15 was cultured in DMEM: F-12 (10565018, Gibco) with 10% fetal calf serum and 1% penicillin-streptomycin. Cells were incubated in a humidified incubator at 37 °C with 5% CO₂. Upon reaching 70% confluence, the cells were washed with phosphate buffer saline solution (PBS; 10010049, Gibco) and harvested with Trypsin (25200072, Gibco) for plasma treatment.

The harvested cells were washed with PBS and diluted to a concentration of $2 \times 10^5/100 \mu\text{L}$. 100 μL cell suspension was transferred to the glass receptacles for plasma exposure. Following treatment, the cell suspension was transferred to a 6-well plate, and 1 mL of fresh culture media was added. The plate was then incubated for 24 h.

To characterize cell proliferation, the old media was replaced with 500 μL of fresh culture media containing 10% WST-8 solution (ab228544, abcam) solution. The cells were incubated at 37 °C in the dark for 40 min. Subsequently, light absorbance was measured by a microreader (SpectraMax iD3, Molecular Devices) at the wavelength of 450 nm.

Bacterial culture and plasma treatment

S. aureus (Newman) and *P. aeruginosa* (Pao1) were purchased from ATCC and cultured in Lysogeny Broth (L3022, Sigma). MRSA and MDRSA, sourced from infected patients at Queen Mary Hospital, were cultured in Brain-Heart Infusion Broth (53286, Millipore). The bacteria were cultured in a shaker incubator until an OD value of 0.5 was reached. These four types of bacteria were diluted with PBS to a concentration of 10^6 CFU/mL.

100 μL bacteria suspension was transferred to the pre-sterilized glass receptacles for direct plasma treatment. The treated solution was then diluted 10-fold with PBS and inoculated onto agar plates for colony counting and observation.

To evaluate the influence of plasma treatment on biofilm formation, 100 μL suspension of *S. aureus* with a density of 10^8 CFU/mL was exposed to plasma for 1 min, 3 min, and 5 min. After treatment, the samples were incubated in the glass receptacles for 48 h at 37 °C with 5% CO₂ to assess biofilm growth.

For live-dead observation, the *S. aureus* was cultured in the receptacles for 24 h before plasma treatment. For SEM observation, *S. aureus* was grown on glass coverslips for 24 h prior to plasma treatment.

Quantification of H₂O₂ and NO₂⁻ generation

H₂O₂ generation in plasma-activated PBS was quantified using the fluorometric H₂O₂ assay kit (MAK165, Sigma-Aldrich). Plasma-activated 50 µL PBS solution was mixed with 50 µL of the working solution prepared according to the manufacturer's instructions. The mixture was incubated in darkness at room temperature for 30 min. Fluorescence intensity was detected using a microplate reader (SpectraMax iD3, Molecular Devices) at the excitation/emission wavelength of 540 nm/590 nm. The concentration of NO₂⁻ in plasma-activated PBS was measured using the Griess Reagent System (G2930, Promega). Following the manufacturer's protocol, 50 µL of plasma-activated PBS solution was first mixed with 50 µL of sulfanilamide solution and incubated in darkness at room temperature for 7 min. Subsequently, 50 µL of NED solution was added to the mixture, which was then incubated in darkness at room temperature for an additional 7 min. Light absorbance was detected using a microplate reader (SpectraMax iD3, Molecular Devices) at a wavelength of 530 nm.

Crystal Violet staining of the bacteria

The biofilm grown in glass receptacles for 48 h was fixed with 2.5% (v/v) glutaraldehyde (G105907, Aladdin) for 2 h. Following fixation, the sample was left in a fume hood overnight to dry completely, then stained with 0.5% (w/v) crystal violet (C0775, Sigma) for 30 min. The stained samples were then washed three times with PBS, dissolved in 30% (v/v) acetic acid (A112880, Aladdin), and the light absorbance was measured using a micro reader at the wavelength of 595 nm.

Live-dead assay of the bacteria

The biofilm grown in the glass receptacles for 24 h was washed with PBS and stained using the Live-dead assay (L34856, Invitrogen) according to the instructions. After staining, the sample was washed with PBS and transferred to a 96-well plate for fluorescence observation.

Sample preparation for SEM observation

After treatment, *S. aureus* grown on glass slides was fixed with 2.5% (v/v) glutaraldehyde for 2 h and dehydrated using a graded series of ethanol (EtOH) concentrations: 30%, 50%, 70%, 90%, 100%, with each concentration for 10 min. The sample was then dried at 37 °C overnight and observed using a scanning electron microscope (SEM; SU1510, Hitachi).

Fluidic and electrical field simulation

The gas flow and electrical field model were constructed using the finite element analysis tool COMSOL Multiphysics 6.0. Due to the relatively low flow speed, laminar flow and stationary calculation were employed. To simplify the

computation, only a quarter part of the model was simulated, taking advantage of model symmetry. Boundary conditions at the inlets and outlets included gas flux and pressure, respectively. A flow flux boundary condition of 500 mL/min was applied at the inlets, and a pressure of 0 MPa relative to the atmospheric pressure was imposed at the outlets. Standard helium gas, as embedded in the software, was used for the calculations. The Navier-stokes equation was utilized to model the flow.

Electrostatic interactions were considered dominant, thus other physical phenomena were excluded from the simulation. We simulated a scenario with no feedstock gas, thus no plasma was generated. The voltage between the positive and negative electrodes was set to the peak of the actual applied voltage, and the potential distribution was analyzed at that moment.

Statistical analysis

Results are presented as means ± SD or as means ± SEM. One-way ANOVA was applied for multiple comparisons. The threshold for statistical significance was set at $P < 0.05$.

Acknowledgements

The authors gratefully acknowledge Dr. Alan Wong (School of Biomedical Sciences, HKU) for providing the Lung cancer cell line A549 and liver cell line Huh7, and Prof. James Kit Hon Tsoi (Faculty of Dentistry, HKU) for providing the tongue cancer cell line of SCC-15 to support this research. This work was supported by the following funding: National Science Foundation of China (NSFC) (62373259); Natural Science Foundation of Top Talent of SZTU (Grant No. GDRC202303); Foundation of Education Department of Guangdong Province, China (Grant No. 2022ZDJS115); National Natural Science Foundation of China (NSFC) (52035009, 52005243); NSFC Excellent Yong Scientists Fund (Hong Kong and Macau, China) (21922816); Science and Technology Innovation Committee of Shenzhen Municipality (JCYJ20200109141003910, JCYJ20210324120402007, KQTD20170810110250357) Platform Technology Funding from the University of Hong Kong; H.C.S. was supported in part by the Croucher Foundation through the Croucher Senior Research Fellowship.

Author details

¹Department of Mechanical Engineering, The University of Hong Kong, Hong Kong SAR, China. ²Department of Mechanical and Energy Engineering, Southern University of Science and Technology, Shenzhen, China. ³College of Health Science and Environmental Engineering, Shenzhen Technology University, Shenzhen, China. ⁴Department of Ophthalmology, The University of Hong Kong, Hong Kong SAR, China. ⁵Advanced Biomedical Instrumentation Centre, Hong Kong Science Park, Shatin, New Territories, Hong Kong SAR, China. ⁶Department of Chemistry and Department of Biomedical Engineering, City University of Hong Kong, Hong Kong SAR, China

Author contributions

Fang Wang conceptualized this article; Fang Wang, Liangyu Zhou, and Xiaoxue Fan performed experiments; Hui Deng and Ho Cheung Shum supervised this work; Fang Wang drafted the manuscript; Fang Wang, Ruotong Zhang, Yuan Liu, Haisong Lin, Wei Guo, Shaolong Kuang, and Yau Kei Chan revised and edited the manuscript.

Data availability

Data will be made available on request.

Conflict of interest

H.C.S. is a scientific advisor of EN Technology Limited in which he owns some equity, and also a managing director of the research center, namely Advanced Biomedical Instrumentation Center Limited. The work in the paper is however not directly related to the works of these two entities, as far as we know.

Supplementary information The online version contains supplementary material available at <https://doi.org/10.1038/s41378-025-00974-8>.

Received: 18 December 2024 Revised: 8 April 2025 Accepted: 6 May 2025
Published online: 16 June 2025

References

- Bruggeman, P. J., Iza, F. & Brandenburg, R. Foundations of atmospheric pressure non-equilibrium plasmas. *Plasma Sources Sci. Technol.* **26**, 123002 (2017).
- Lu, X. et al. Reactive species in non-equilibrium atmospheric-pressure plasmas: Generation, transport, and biological effects. *Phys. Rep.* **630**, 1–84 (2016).
- Kumar Dubey, S. et al. Emerging innovations in cold plasma therapy against cancer: a paradigm shift. *Drug Discov. Today* **27**, 2425–2439 (2022).
- Min, T. et al. Therapeutic effects of cold atmospheric plasma on solid tumor. *Front. Med.* **9**, 884887 (2022).
- Dai, X., Bazaka, K., Richard, D. J., Thompson, E. R. W. & Ostrikov, K. K. The emerging role of gas plasma in oncology. *Trends Biotechnol.* **36**, 1183–1198 (2018).
- Zhang, H., Zhang, C. & Han, Q. Mechanisms of bacterial inhibition and tolerance around cold atmospheric plasma. *Appl. Microbiol. Biotechnol.* **107**, 5301–5316 (2023).
- Murali, R. et al. Cold atmospheric plasma (CAP) in wound healing: harnessing a dual-edged sword. *Redox Exp. Med.* **2024**, e230026 (2024).
- Bekeschus, S., Von Woedtke, T., Emmert, S. & Schmidt, A. Medical gas plasma-stimulated wound healing: Evidence and mechanisms. *Redox Biol.* **46**, 102116 (2021).
- Dubey, S. K. et al. Cold atmospheric plasma therapy in wound healing. *Process Biochem.* **112**, 112–123 (2022).
- Cheng, H., Xu, J., Li, X., Liu, D. & Lu, X. On the dose of plasma medicine: equivalent total oxidation potential (ETOP). *Phys. Plasmas* **27**, 063514 (2020).
- Cheng, H. et al. On the dose of plasma medicine: plasma-activated medium (PAM) and its effect on cell viability. *Phys. Plasmas* **29**, 063506 (2022).
- Dai, X., Zhang, Z., Zhang, J. & Ostrikov, K. Dosing: the key to precision plasma oncology. *Plasma Process. Polym.* **17**, e1900178 (2020).
- Yan, D., Horkowitz, A., Wang, Q. & Keidar, M. On the selective killing of cold atmospheric plasma cancer treatment: status and beyond. *Plasma Process. Polym.* **18**, e2100020 (2021).
- Abdo, A. I. & Kopecki, Z. Comparing redox and intracellular signalling responses to cold plasma in wound healing and cancer. *Curr. Issues Mol. Biol.* **46**, 4885–4923 (2024).
- Corbella, C., Portal, S. & Keidar, M. Flexible cold atmospheric plasma jet sources. *Plasma* **6**, 72–88 (2023).
- Maho, T. et al. Anti-bacterial action of plasma multi-jets in the context of chronic wound healing. *Appl. Sci. -Basel* **11**, 9598 (2021).
- Lin, A. et al. Non-thermal plasma as a unique delivery system of short-lived reactive oxygen and nitrogen species for immunogenic cell death in melanoma cells. *Adv. Sci.* **6**, 1802062 (2019).
- Do Nascimento, F. et al. Plasma electrode dielectric barrier discharge: development, characterization and preliminary assessment for large surface decontamination. *Plasma Chem. Plasma Process.* **43**, 1791–1817 (2023).
- Hou, J. et al. Non-thermal plasma treatment altered gene expression profiling in non-small-cell lung cancer A549 cells. *BMC Genom.* **16**, 435 (2015).
- Chen, G. et al. Portable air-fed cold atmospheric plasma device for postsurgical cancer treatment. *Sci. Adv.* **7**, eabg5686 (2021).
- Chen, G. et al. Transdermal cold atmospheric plasma-mediated immune checkpoint blockade therapy. *Proc. Natl Acad. Sci. USA* **117**, 3687–3692 (2020).
- Bekeschus, S. et al. Medical gas plasma jet technology targets murine melanoma in an immunogenic fashion. *Adv. Sci.* **7**, 1903438 (2020).
- Lin, L. & Keidar, M. A map of control for cold atmospheric plasma jets: from physical mechanisms to optimizations. *Appl. Phys. Rev.* **8**, 011306 (2020).
- He, W. et al. Gas diffusion mechanisms and models. in *Gas Transport in Solid Oxide Fuel Cells* 9–17 (Springer International Publishing, 2014).
- Baek, E. J., Joh, H. M., Kim, S. J. & Chung, T. Effects of the electrical parameters and gas flow rate on the generation of reactive species in liquids exposed to atmospheric pressure plasma jets. *Phys. Plasmas* **23**, 1–9 (2016).
- Humud, H. R., Abbas, Q. A. & Rauuf, A. F. Effect of gas flow rate on the electron temperature, electron density and gas temperature for atmospheric microwave plasma jet. *Int. J. Curr. Eng. Technol.* **5**, 2277–4106 (2015).
- Bauer, G. The synergistic effect between hydrogen peroxide and nitrite, two long-lived molecular species from cold atmospheric plasma, triggers tumor cells to induce their own cell death. *Redox Biol.* **26**, 101291 (2019).
- Yan, D., Sherman, J. H. & Keidar, M. Cold atmospheric plasma, a novel promising anti-cancer treatment modality. *Oncotarget* **8**, 15977–15995 (2017).
- von Woedtke, T., Laroussi, M. & Gherardi, M. Foundations of plasmas for medical applications. *Plasma Sources Sci. Technol.* **31**, 054002 (2022).
- Sgouros, G., Bodei, L., McDevitt, M. R. & Nedrow, J. R. Radiopharmaceutical therapy in cancer: clinical advances and challenges. *Nat. Rev. Drug Discov.* **19**, 589–608 (2020).
- Wang, X., Zhong, X., Liu, Z. & Cheng, L. Recent progress of chemodynamic therapy-induced combination cancer therapy. *Nano Today* **35**, 100946 (2020).
- Mitra, S. et al. Impact of ROS generated by chemical, physical, and plasma techniques on cancer attenuation. *Cancers* **11**, 1030 (2019).
- Keidar, M. Plasma for cancer treatment. *Plasma Sources Sci. Technol.* **24**, 033001 (2015).
- Nedeljkovic, M. & Damjanovic, A. Mechanisms of chemotherapy resistance in triple-negative breast cancer-how we can rise to the challenge. *Cells* **8**, 957 (2019).
- Koritzer, J. et al. Restoration of sensitivity in chemo-resistant glioma cells by cold atmospheric plasma. *Plos One* **8**, e64498 (2013).
- Gan, L. et al. Cold atmospheric plasma applications in dermatology: a systematic review. *J. Biophotonics* **14**, e202000415 (2021).
- Chen, Z. et al. Cold atmospheric plasma delivery for biomedical applications. *Mater. Today* **54**, 153–188 (2022).
- McDonald, E. M., Ram, F. S., Patel, D. V. & McGhee, C. N. Topical antibiotics for the management of bacterial keratitis: an evidence-based review of high quality randomised controlled trials. *Br. J. Ophthalmol.* **98**, 1470–1477 (2014).
- Karin Jepsen, S. J. Antibiotics/antimicrobials: systemic and local administration in the therapy of mild to moderately advanced periodontitis. *Periodontology* **71**, 82–112 (2016).
- Negut, I., Grumezescu, V. & Grumezescu, A. M. Treatment strategies for infected wounds. *Molecules* **23**, <https://doi.org/10.3390/molecules23092392> (2018).
- Darby, E. M. et al. Molecular mechanisms of antibiotic resistance revisited. *Nat. Rev. Microbiol.* **21**, 280–295 (2023).
- Lu, X. et al. Transcutaneous plasma stress: from soft-matter models to living tissues. *Mater. Sci. Eng. R Rep.* **138**, 36–59 (2019).
- Hammudi, R. A., Hammudi, Y. A. & Ghnaimawi, S. The important role of cold atmospheric plasma in wounds healing. *J. Sci. Technol. Environ.* **13**, 49–55 (2024).
- Murali, R. et al. Cold atmospheric plasma (CAP) in wound healing: harnessing a dual-edged sword. *Redox Exp. Med.* **2024**, <https://doi.org/10.1530/rem-23-0026> (2023).
- Dai, X., Bazaka, K., Thompson, E. W. & Ostrikov, K. K. Cold atmospheric plasma: a promising controller of cancer cell states. *Cancers* **12**, 3360 (2020).
- Rispin, A. et al. Alternative methods for the median lethal dose (LD50) test: the up-and-down procedure for acute oral toxicity. *ILAR J.* **43**, 233–243 (2002).
- Gupta, T. T. & Ayan, H. Application of non-thermal plasma on biofilm: a review. *Appl. Sci.* **9**, 3548 (2019).
- Zhou, R. et al. Plasma-activated water: generation, origin of reactive species and biological applications. *J. Phys. D Appl. Phys.* **53**, 303001 (2020).
- Szili, E. J., Hong, S.-H., Oh, J.-S., Gaur, N. & Short, R. D. Tracking the penetration of plasma reactive species in tissue models. *Trends Biotechnol.* **36**, 594–602 (2018).
- Wang, F. et al. A composition-tunable cold atmospheric plasma chip for multiplex-treatment of cells. *Lab Chip* **23**, 580–590 (2023).
- Yan, W. & Economou, D. J. Gas flow rate dependence of the discharge characteristics of a helium atmospheric pressure plasma jet interacting with a substrate. *J. Phys. D Appl. Phys.* **50**, <https://doi.org/10.1088/1361-6463/aa8794> (2017).
- Gorbanev, Y., Privat-Maldonado, A. & Bogaerts, A. Analysis of short-lived reactive species in plasma-air-water systems: the dos and the do nots. *Anal. Chem.* **90**, 13151–13158 (2018).
- Liu, K. et al. Long-lived species in plasma-activated water generated by an AC multi-needle-to-water discharge: effects of gas flow on chemical reactions. *J. Phys. D Appl. Phys.* **54**, <https://doi.org/10.1088/1361-6463/abc211> (2020).